Diagn Interv Radiol 2016; 22:161–167

HEAD AND NECK IMAGING

ORIGINAL ARTICLE

Utility of histogram analysis of ADC maps for differentiating orbital tumors

Xiao-Quan Xu*
Hao Hu*
Guo-Yi Su
Hu Liu
Xun-Ning Hong
Hai-Bin Shi
Fei-Yun Wu

PURPOSE
We aimed to evaluate the role of histogram analysis of apparent diffusion coefficient (ADC) maps for differentiating benign and malignant orbital tumors.

METHODS
Fifty-two patients with orbital tumors were enrolled from March 2013 to November 2014. Pretreatment diffusion-weighted imaging was performed on a 3T magnetic resonance scanner with b factors of 0 and 800 s/mm^2, and the corresponding ADC maps were generated. Whole-tumor regions of interest were drawn on all slices of the ADC maps to obtain histogram parameters, including ADC_{mean}, ADC_{median}, standard deviation (SD), skewness, kurtosis, quartile, ADC_{10}, ADC_{25}, ADC_{75}, and ADC_{90}. Histogram parameter differences between benign and malignant orbital tumors were compared. The diagnostic value of each significant parameter in predicting malignant tumors was established.

RESULTS
Age, ADC_{mean}, ADC_{median}, quartile, kurtosis, ADC_{10}, ADC_{25}, ADC_{75}, and ADC_{90} parameters were significantly different between benign and malignant orbital tumor groups, while gender, location, SD, and skewness were not significantly different. The best diagnostic performance in predicting malignant orbital tumors was achieved at the threshold of ADC_{10}=0.990 (AUC, 0.997; sensitivity, 96.2%; specificity, 100%).

CONCLUSION
Histogram analysis of ADC maps holds promise for differentiating benign and malignant orbital tumors. ADC_{10} has the potential to be the most significant parameter for predicting malignant orbital tumors.

Accurate differentiation of malignant and benign orbital tumors before surgery is critical in tumor diagnosis and treatment planning (1). Such differentiation is commonly performed based on typical imaging features, and it works well for some particular orbital tumors, including cavernous malformation, venous varix, lymphangioma, and orbital cyst (2, 3). However, characterization of other orbital tumors without typical imaging features remains a challenge.

Recently, diffusion-weighted imaging (DWI), which allows characterization of diffusion of water molecules in tumor tissues, has shown promise for differentiating malignant and benign orbital tumors (4–12). Due to their relatively high cellularity and limited extracellular space, malignant tumors commonly show high signal intensity on DWI and yield low apparent diffusion coefficient (ADC) values. In previous studies, the mean ADC value was used as a differentiating parameter (9–12). However, the mean ADC value has a substantial overlap between benign and malignant tumors, which limits its clinical value in tumor differentiation for individual patients (9–12). This overlap may be a result of the mean ADC value being the average value of whole regions of interest (ROIs) in tumor tissues, which does not reveal the heterogeneity of tumor tissues.

As a novel technique to analyze the parametric maps, histogram analysis based on pixel distribution can provide quantitative information about tumor heterogeneity. This method has demonstrated its superiority in differentiating and grading tumors or predicting treatment response in various organs (13–18). However, to the best of our knowledge, no study has used the histogram analysis of ADC maps in differentiating benign and malignant orbital tumors until now. In addition, previous DWI-based studies mostly used the one-slice

* These authors contributed equally to this work.

From the Departments of Radiology (X.Q.X., H.H., G.Y.S., X.N.H., H.B.S., F.Y.W. ✉ *wfy_njmu@163.com*), and Ophthalmology (H.L.), The First Affiliated Hospital of Nanjing Medical University, Nanjing, China.

Received 15 May 2015; revision requested 16 June 2015; revision received 1 July 2015; accepted 8 August 2015.

Published online 1 February 2016.
DOI 10.5152/dir.2015.15202

ROI approach that places ROI on a representative section of the tumor, which is subjective and prone to sampling bias (14, 17). A whole-tumor ROI approach that encompasses the entire tumor, would provide more information about the heterogeneity of the tumor, thus it can potentially eliminate sampling bias during data processing (13, 16, 17, 19).

Therefore, the aim of our study was to evaluate the value of histogram analysis of ADC maps in differentiating benign and malignant orbital tumors, by using the whole-tumor ROI approach.

Methods

Patients

Our retrospective study protocol was reviewed and approved by the institutional review board of our hospital. The requirement for written informed consent was waived due to the retrospective nature of the study. A retrospective review of our institution's database identified 91 consecutive patients who had undergone DWI scan for pretreatment evaluation of orbital tumors from March 2013 to November 2014. First, similar to previous studies that used DWI to differentiate benign and malignant orbital tumors, patients with cavernous malformation (n=20), lymphangioma (n=1), venous varix (n=4), and epidermoid cyst (n=5) were excluded because of their characteristic findings on routine magnetic resonance imaging (MRI) (2, 10). Additionally, four patients were excluded because the largest diameter of the lesion was less than 1 cm and five patients were excluded because of poor image quality. Finally, we enrolled 52 patients, including 26 patients with benign orbital tumors and 26 patients with malignant orbital tumors. The male/female ratio was 29:23. The mean patient age was 50.4±15.6 years (range, 18–90 years).

Main points

- Histogram parameters, including ADC_{mean}, ADC_{median}, quartile, kurtosis, ADC_{10}, ADC_{25}, ADC_{75}, and ADC_{90}, were significantly different between benign and malignant orbital tumor groups.
- No significant difference on standard deviation and skewness were found between benign and malignant orbital tumor groups.
- The ADC_{10} was the most promising parameter for predicting the malignant orbital tumors.
- Histogram analysis of ADC maps could effectively show the heterogeneity of orbital lesions, and help differentiate benign and malignant tumors.

Twenty-six benign orbital masses comprised inflammatory pseudotumor (n=9), pleomorphic adenoma of the lacrimal gland (n=7), schwannoma (n=5), optic nerve sheath meningioma (n=4), and solitary fibrous tumor (n=1). Twenty-six malignant orbital masses comprised lymphoma (n=18), metastases (n=2), adenoid cystic carcinoma (n=2), basocellular carcinoma (n=1), lymphoepithelial carcinoma (n=1), Ewing sarcoma (n=1), and melanoma (n=1).

The final diagnosis of orbit tumors was made based on pathologic examination after surgical excision in 47 patients, typical imaging finding and long-term follow-up in two patients with optic nerve sheath meningioma, and follow-up after treatment in three patients with orbital inflammatory pseudotumor.

Magnetic resonance imaging

MRI examinations were performed with a 3T scanner (Verio, Siemens Medical System) using a 12-channel head coil. Routine imaging protocols included unenhanced axial T1-weighted imaging (repetition time [TR]/echo time [TE], 600/10 ms), axial T2-weighted imaging (TR/TE, 4700/79 ms) with fat saturation, coronal T2-weighted imaging (TR/TE, 3500/79 ms), and contrast-enhanced axial T1-weighted imaging (TR/TE, 500/10 ms). For contrast-enhanced axial T1-weighted imaging, a standard dose of 0.1 mmol/kg of gadolinium-diethylene triamine pentaacetic acid (Magnevist, Bayer Schering Pharma AG) was administrated at a rate of 4 mL/s, followed by a 20 mL bolus of saline with the same injection rate.

A standard single-shot spin-echo echo-planar imaging sequence was routinely used for DWI scan with two b values (0 and 800 s/mm^2) in three orthogonal directions. The imaging parameters were as follows: TR/TE, 4000/85 ms; flip angle, 150°; number of averages, 6; field of view, 200×200 mm; slice thickness, 4 mm without gap; matrix, 384×384; number of sections, 10. The total acquisition time of DWI was 4 min 14 s.

Image processing

All DWI data with Digital Imaging and Communication in Medicine (DICOM) format was transferred from the picture archiving and communication system (PACS) workstation (Centricity PACS 3.1.1.4, GE Healthcare) to an independent, personal computer for further analysis. The images were processed with Image J software (http://rsbweb.nih.gov/ij/). All ROIs were drawn on all imaging sections to encompass the entire tumor area, with exclusion of large necrotic, cystic, and hemorrhagic areas and surrounding blood vessels. T2-weighted and contrast-enhanced T1-weighted images were used as reference to determine tumor areas. The ROIs were slightly smaller in size than actual tumor size to reduce the influence of partial volume effect. In patients with bilateral lesions, only the relative larger lesion was included in the analysis. Once the ROIs were determined, histogram analysis was performed. The parameters derived from histogram analysis included: ADC_{mean}, ADC_{median}, standard deviation (SD), skewness, and kurtosis. Kurtosis, is a measure of the peakedness of the histogram: the value is equal to 3 when the histogram is Gaussian, >3 with a sharper peak, and <3 with a flatter top. Skewness, which is a measure of the asymmetry of the histogram, is positive if the majority of the data is concentrated on the left of the histogram and negative if the majority of data is concentrated on the right. We also measured four cumulative histogram parameters including the 10th (ADC_{10}), 25th (ADC_{25}), 75th (ADC_{75}), 90th (ADC_{90}) percentiles of ADC, and quartile. The *n*th percentile was the point at which *n*% of the voxel values that form the histogram were found to the left (13). The quartile means the difference between ADC_{25} and ADC_{75}.

All ROIs were contoured by two radiologists (reader 1, with 14 years of clinical experience in head and neck radiology; reader 2, with three years of clinical experience in head and neck radiology). The measurements of the two radiologists were used to calculate interreader reproducibility. To assess the intrareader reproducibility, the first reader re-assessed all the images, which were presented in a different order, one month after the first assessment. The average of the two measurements of the first reader was used in statistical analysis.

Statistical analysis

Numeric data were averaged over all patients and reported as mean±SD. The Kolmogorov-Smirnov's test was used to determine whether the quantitative parameters were normally distributed. The differences of gender and tumor location between benign and malignant groups were compared

using the chi-square test. Age difference and the difference of histogram parameters between the two groups were compared with unpaired t test. Receiver operating characteristic (ROC) curve was performed to determine the diagnostic value of significant parameters to differentiate malignant from benign orbital tumors. Cutoff values were established by calculating the maximal Youden index (Youden index = sensitivity + specificity-1).

The intraclass correlation coefficient (ICC) with 95% confidence intervals (CI) was used to evaluate the inter- and intrareader agreement of quantitative assessment of MRI, respectively. The ICC ranged between 0 and 1.00, and values closer to 1.00 meant better reproducibility. They were interpreted as follows: <0.40, poor; 0.41–0.60, moderate; 0.61–0.80, good; ≥0.81, excellent. $P < 0.05$ indicated statistical significance. Statistical analysis was carried out using software package (SPSS v. 19.0, IBM corp.)

Results

There were 26 patients with benign tumors (15 males and 11 females; mean age 45.5±13.5 years; range, 26–70 years) and 26 patients with malignant tumors (14 males and 12 females; mean age 55.3±16.2 years; range, 18–90 years). In the benign group, unilateral orbit was involved in 24 patients and bilateral orbits were involved in two patients. In the malignant group, unilateral orbit was involved in 23 patients and bilateral orbits were involved in three patients. There was no significant difference in gender distribution of patients ($P = 0.619$) and location of orbital tumors ($P = 0.638$) between benign and malignant groups, while age of patients was significantly different between the two groups ($P = 0.021$). The demographic characteristics of all patients are summarized in Table 1.

The ADC_{mean} ($P < 0.0001$), ADC_{median} ($P < 0.0001$), ADC_{10} ($P < 0.0001$), ADC_{25} ($P < 0.0001$), ADC_{75} ($P < 0.0001$), ADC_{90} ($P < 0.0001$), quartile ($P = 0.0001$), and kurtosis ($P = 0.0048$) were found to be significantly different between benign and malignant groups, while there was no significant difference on the SD ($P = 0.1797$) and skewness ($P = 0.8548$). Detailed histogram parameters of benign and malignant orbital tumors are summarized in Table 2. Comparison of histogram parameters from ADC maps between benign and malignant orbital tumors is shown in box plots (Fig. 1). Representative cases of orbit lymphoma and inflammatory pseudotumor are presented in Figs. 2 and 3, respectively.

ROC analysis results indicated that when ADC_{10}=0.990 was set as the threshold value, the best diagnostic performance in predicting malignant tumors was achieved (AUC, 0.997; sensitivity, 96.2%; specificity, 100%), followed by ADC_{25}, ADC_{median}, ADC_{75}, ADC_{mean}, ADC_{90}, quartile, and kurtosis. Detailed diagnostic performance of histogram parameters are summarized in Table 3. ROC curve of using ADC_{10} to differentiate benign and malignant orbital tumors is shown in Fig. 4.

Inter- and intrareader agreement was excellent for the measurements of histogram parameters, with interreader ICCs values ranging from 0.839 to 0.893 and intrareader ICCs values ranging from 0.856 to 0.913, respectively. Detailed inter- and intrareader ICCs for the measurements of histogram parameters are presented in Table 4.

Discussion

Our study indicated that histogram parameters are significantly different between benign and malignant orbital tumor groups. Histogram analysis of ADC maps could effectively demonstrate the heterogeneity of orbital tumors, and help differentiate benign and malignant tumors. The ADC_{10} might be the most promising parameter for predicting the malignant orbital tumors. To the best of our knowledge, our study was the first one to use the histogram analysis of ADC maps to differentiate benign and malignant orbital tumors.

DWI is currently used in routine clinical practice for preoperative differentiating

Table 1. Demographic data of all patients

Demographic data	Benign group (n=26)	Malignant group (n=26)	*P*
Mean age	45.5±13.5	55.3±16.2	0.021
Gender (F/M)	11/15	12/14	0.619
Location (U/B)	24/2	23/3	0.638
Diagnosis	Inflammatory pseudotumor (9)	Lymphoma (18)	-
	Pleomorphic adenoma (7)	Adenoid cystic carcinoma (2)	
	Schwannoma (5)	Metastases (2)	
	Optic nerve sheath meningioma (4)	Basocellular carcinoma (1)	
	Solitary fibrous tumor (1)	Lymphoepithelial carcinoma (1)	
		Ewing sarcoma (1)	
		Melanoma (1)	

Data in parentheses indicate the number of corresponding patients in our study.
F, female; M, male; U, unilateral; B, bilateral.

Table 2. Difference of histogram parameters between benign and malignant subgroups

Parameter	Benign group	Malignant group	*P*
ADC_{mean}	1.934±0.374	0.821±0.293	<0.001
SD	0.309±0.118	0.247±0.201	0.1797
ADC_{Median}	1.879±0.372	0.780±0.236	<0.001
ADC_{10}	1.578±0.316	0.579±0.228	<0.001
ADC_{25}	1.720±0.352	0.671±0.218	<0.001
ADC_{75}	2.145±0.422	0.916±0.270	<0.001
ADC_{90}	2.349±0.480	1.113±0.501	<0.001
Quartile	0.425±0.181	0.245±0.123	<0.001
Kurtosis	0.273±0.800	1.890±2.675	0.0048
Skewness	0.599±0.541	0.637±0.908	0.8548

Data are presented as mean±SD.
The unit for ADC value is $\times 10^{-3}$ mm^2/s.
SD, standard deviation; ADC, apparent diffusion coefficient; ADCn, nth percentile value of cumulative ADC histogram.

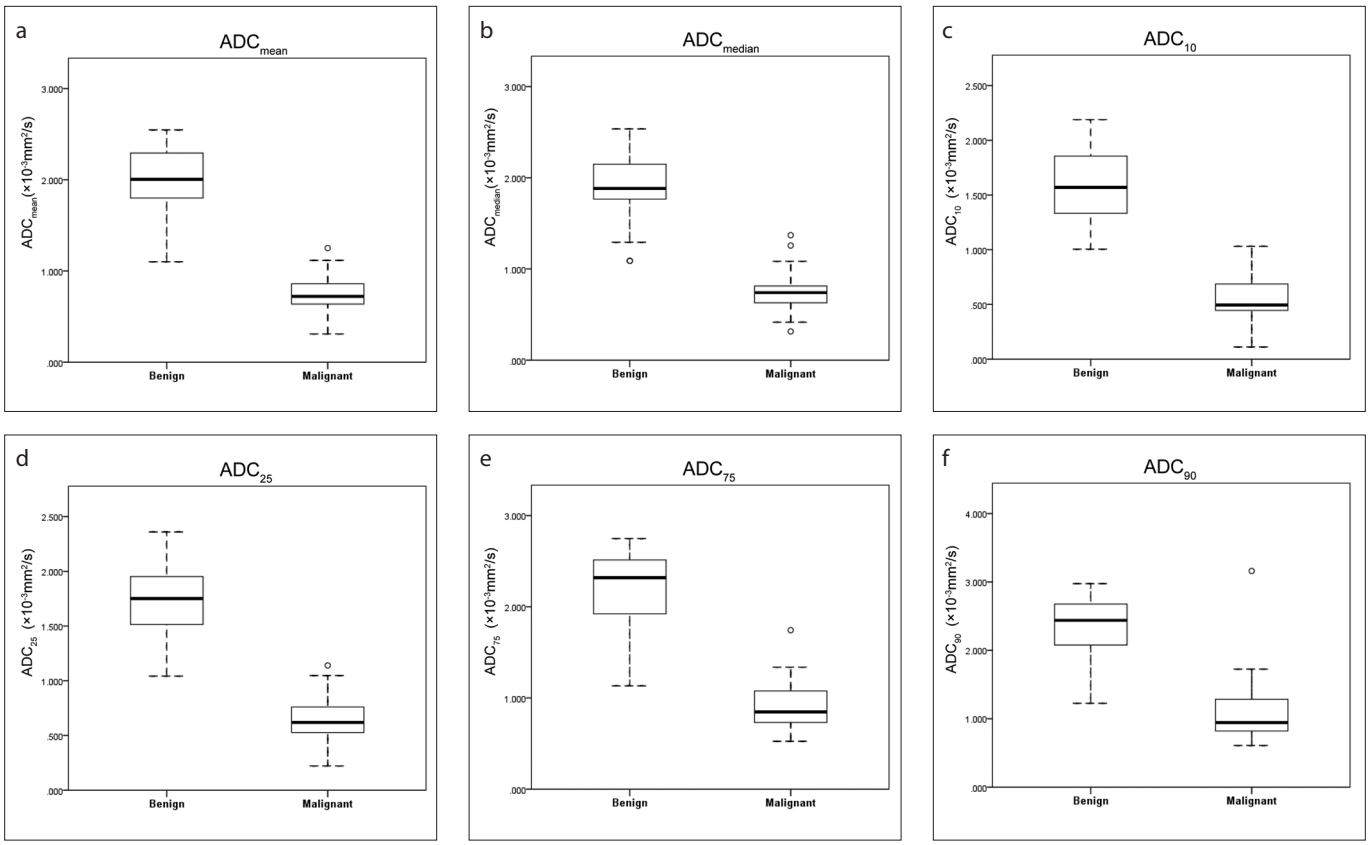

Figure 1. a–f. Box plots show comparison of ADC parameters for benign and malignant orbital tumors. Line in box represents the median, height of the box represents the interquartile range, whiskers are the lowest and highest data points within 1.5 interquartile range, and circles indicate outliers.

Table 3. Diagnostic performance of each significant histogram parameter for differentiating benign orbital tumors from malignant tumors

Parameters	AUC	Cutoff value ($\times 10^{-3}$ mm^2/s)	Sensitivity (100%)	Specificity (100%)
Mean	0.981 (0.953–1.000)	1.314	0.962	0.923
Median	0.991 (0.975–1.000)	1.087	0.923	1.000
ADC_{10}	0.997 (0.989–1.000)	0.990	0.962	1.000
ADC_{25}	0.994 (0.982–1.000)	1.012	0.923	1.000
ADC_{75}	0.982 (0.956–1.000)	1.451	0.962	0.923
ADC_{90}	0.941 (0.862–1.000)	1.745	0.962	0.923
Quartile	0.812 (0.685–0.939)	0.297	0.808	0.808
Kurtosis	0.800 (0.676–0.925)	0.341	0.731	0.808

Data in parentheses indicate 95% confidence intervals.
AUC, area under the ROC curve; ADC, apparent diffusion coefficient; ADCn, nth percentile value of cumulative ADC histogram.

and grading various tumors. However, the commonly used average ADC measurement ignores the heterogeneity of the tumors, which is an important characteristic of both benign and malignant tumors. Due to its ability to analyze lesions pixel by pixel, histogram analysis was regarded as an effective method to deal with this problem (13–23). In a recent study, Donati et al. (20) found that the 10th percentile ADC value correlated with Gleason score, suggesting the 10th percentile ADC value could help differentiate low-grade from intermediate or high-grade prostate cancer. In another study, Heo et al. (21) found that the 75th percentile ADC value of tumors was a significant predictor for tumor recurrence in patients with uterine cervical cancer after chemoradiation therapy. However, while histogram analysis of ADC maps has been successfully used in various organs, its utility in orbital disease has not been reported yet.

In our study, the mean ADC value of malignant orbit tumors was significantly lower than that of the benign tumors, which was similar to previous studies (10–12). The reason for this might be hypercellularity, enlarged nuclei, and reduced extracellular space in malignant tumors. Meanwhile, we found that malignant orbital tumors have a significantly higher kurtosis than benign tumors. In our opinion, this can be explained by the composition of our patients. Lymphoma was the most common orbital tumor in our patient population, and the most distinctive feature of lymphoma is tumor homogeneity (23, 24). As we know, kurtosis is an important index reflecting the degree of homogeneity of the tumors (14, 19, 25). Therefore, it is not surprising that malignant orbital tumors have a significantly higher kurtosis than benign tumors. Nevertheless, there was no difference on skewness between benign and malignant orbital tumor groups. When we placed the ROIs, only the solid portion of the tumors were selected, while the visual necrotic, cystic areas, and surrounding blood vessels

were all excluded. Because all the areas that demonstrated relatively higher ADC values were excluded, the histogram data concentrated mostly to the left of the histogram in both groups. Therefore, the skewness values were positive in both groups, and no significant difference was found between the two groups.

Previously, some studies found that the low percentile of ADC was better in differentiating or grading tumors than the high percentile of ADC. Kang et al. (26) reported that the minimum ADC and ADC_5 were promising parameters for differentiating high from low grade brain glioma, especially for the ADC value derived from high b value DWI. Similarly, Lu et al. (27) also found that the minimum ADC, ADC_5, and ADC_{10} could help differentiate primary central nervous system lymphomas from tumefactive demyelinating lesions, while ADC_{mean} could not. Similarly, our study results indicated that ADC_{10} was most valuable in predicting malignant orbital tumors. We considered that the high percentile of ADC value was more easily affected by the cystic area in the tumor tissue. As we know, the cystic area is commonly seen in both benign and malignant orbital tumors, such as the Antoni B area in schwannoma, or the microcystic area in malignant tumors like adenoid cystic carcinoma (24). The low percentile of ADC value corresponds well with the densely packed solid component of the tumor tissue (27). It is well known that the characteristic pathological finding of lymphoma is the homogeneous

Table 4. Inter- and intrareader ICCs for measurements of histogram parameters

Parameter	Interreader ICC	Intrareader ICC
Mean	0.893 (0.796–0.940)	0.913 (0.809–0.959)
SD	0.847 (0.747–0.892)	0.881 (0.756–0.946)
Median	0.888 (0.786–0.937)	0.911 (0.801–0.951)
ADC_{10}	0.883 (0.756–0.934)	0.906 (0.795–0.952)
ADC_{25}	0.879 (0.748–0.918)	0.902 (0.779–0.947)
ADC_{75}	0.880 (0.749–0.921)	0.904 (0.780–0.949)
ADC_{90}	0.875 (0.741–0.912)	0.896 (0.800–0.946)
Quartile	0.881 (0.743–0.918)	0.905 (0.794–0.950)
Kurtosis	0.842 (0.743–0.891)	0.876 (0.751–0.936)
Skewness	0.839 (0.723–0.887)	0.856 (0.742–0.899)

Data in parentheses indicate 95% confidence intervals.
ICC, intraclass correlation coefficient; SD, standard deviation; ADC, apparent diffusion coefficient; ADCn, nth percentile value of cumulative ADC histogram.

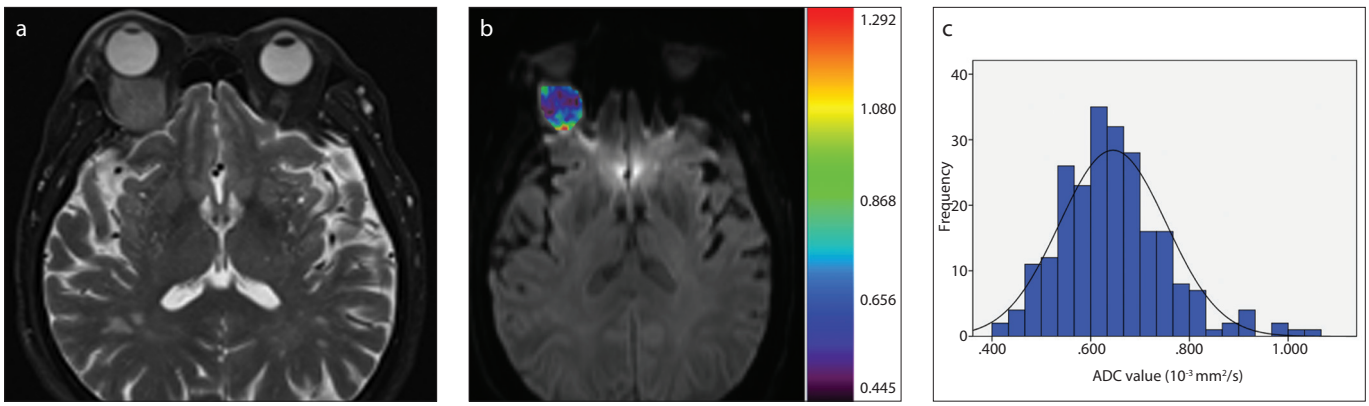

Figure 2. a–c. A 74-year-old man with right orbital lymphoma. Axial T2-weighted image **(a)** shows a lymphoma involving the right orbit. Pixel-by-pixel colored ADC map **(b)** was obtained after selecting the ROI, and then embedded with the axial DWI. The corresponding histogram of the lymphoma **(c)** shows a significant lower cumulative ADC value, but higher relative frequency.

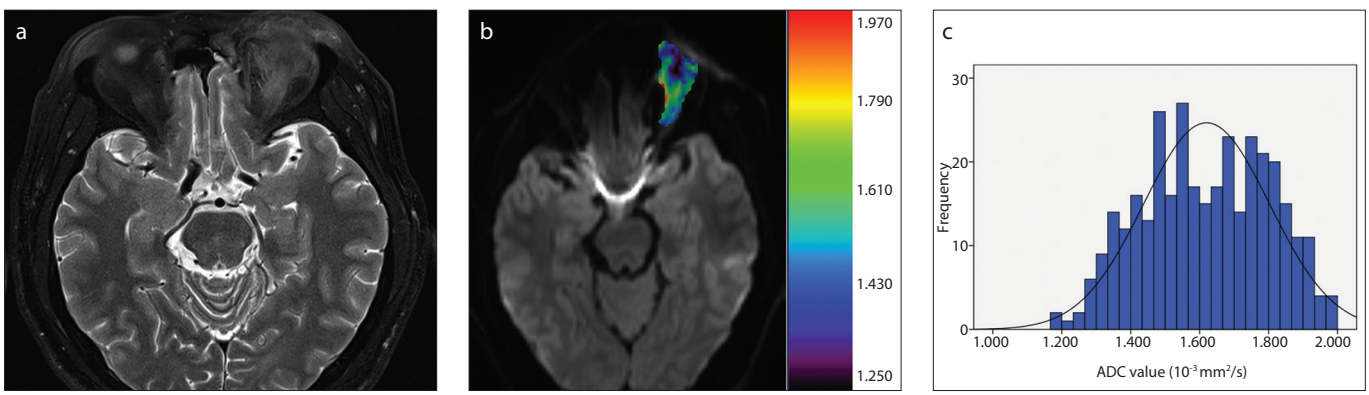

Figure 3. a–c. A 37-year-old man with left orbital inflammatory pseudotumor. Axial T2-weighted image **(a)** shows an inflammatory pseudotumor involving the left orbit. Pixel-by-pixel colored ADC maps **(b)** were obtained after selecting the ROI, and then embedded with the axial DWI. The corresponding histogram of the inflammatory pseudotumor **(c)** shows a relatively higher cumulative ADC value, but lower relative frequency.

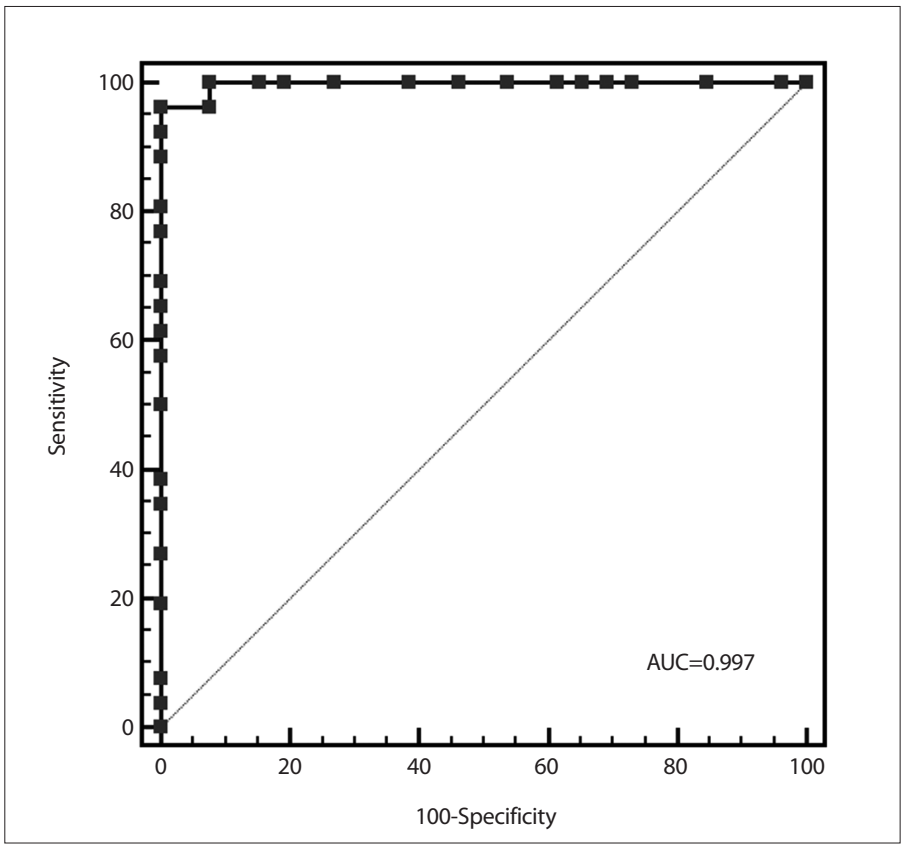

Figure 4. ROC curves of ADC_{10} for differentiation of benign from malignant orbital tumors. The best diagnostic performance in predicting malignant tumors could be achieved at ADC_{10}=0.990 as the threshold (AUC, 0.997; sensitivity, 96.2%; specificity, 100%).

and densely packed lymphoid cell. Meanwhile lymphoma was the most common orbital malignant tumor. Therefore, the low percentile of ADC value would demonstrate better performance than the high percentile of ADC value.

In the present study, whole-tumor ROI approach was used during the imaging process. The majority of previous studies used one or a few selected ROIs when histogram analysis was performed (14, 17). The selection of a localized area in the tumor could be subjective and prone to sampling bias. Considering that the histogram parameters, such as kurtosis, reflect how the data are distributed and how heterogeneous the data is, it would be more reliable to perform histogram analysis with the whole-tumor ROI rather than using one or several selected ROIs. Meanwhile, in our opinion, whole-tumor ROI approach could improve the reproducibility of parameter measurement, which will prompt further clinical application of histogram analysis. In addition, the patients of cavernous malformation, venous varix, epidermoid cyst, and lymphangioma were excluded in our study because of their typical imaging features. These typical imaging features facilitate their differentiation, and additional use of DWI would not further improve the diagnostic accuracy. Therefore, we excluded these patients, in accordance with previous studies (2, 10).

Our study had several limitations. First, although we tried to improve the imaging quality by increasing the numbers of average, nearly 5% of DWI studies were not interpretable due to the susceptibility artifacts. Further improvement of the imaging quality of DWI would be necessary for the study of orbital tumors. Periodically rotated overlapping parallel lines with enhanced reconstruction (PROPELLER) technique or half-Fourier acquired single-shot turbo spin-echo (HASTE) DWI sequence might be the choice in reducing these artifacts (7, 10). Second, we performed the DWI scan using b=800 s/mm^2. However, most previous head and neck studies performed DWI scan using b=1000 s/mm^2. Therefore the threshold value obtained in the study would not be valid for other studies that used b=1000 s/mm^2. Third, we must admit that the sample size, especially the number of the patients with inflammatory pseudotumor was relatively small. However, in our opinion our study could be an important base for further prospective studies. Further studies with larger study populations, especially subgroup analysis of the difference between inflammatory pseudotumor and lymphoma would be clinically important.

In conclusion, our preliminary results indicate that histogram parameters of ADC map are significantly different between the benign and malignant orbital tumor groups. Histogram analysis of ADC maps could effectively show the heterogeneity of orbital tumors, and help differentiate benign and malignant tumors. The ADC_{10} might be the most promising parameter for predicting the malignant orbital tumors.

Conflict of interest disclosure

The authors declared no conflicts of interest.

References

1. Goh PS, Gi MT, Charlton A, et al. Review of orbital imaging. Eur J Radiol 2008; 66:387–395. [CrossRef]
2. Xian J, Zhang Z, Wang Z, et al. Value of MR imaging in the differentiation of benign and malignant orbital tumors in adults. Eur Radiol 2010; 20:1692–1702. [CrossRef]
3. Ben Simon GJ, Annunziata CC, Fink J, et al. Rethinking orbital imaging establishing guidelines for interpreting orbital imaging studies and evaluating their predictive value in patients with orbital tumors. Ophthalmology 2005; 112:2196–2207. [CrossRef]
4. Xu XQ, Cheng QG, Zu QQ, et al. Comparative study of the relative signal intensity on DWI, FLAIR, and T2 images in identifying the onset time of stroke in an embolic canine model. Neurol Sci 2014; 35:1059–1065. [CrossRef]
5. Sepahdari AR, Aakalu VK, Kapur R, et al. MRI of orbital cellulitis and orbital abscess: the role of diffusion-weighted imaging. AJR Am J Roentgenol 2009; 193:W244–250. [CrossRef]
6. Kapur R, Sepahdari AR, Mafee MF, et al. MR imaging of orbital inflammatory syndrome, orbital cellulitis, and orbital lymphoid lesions: the role of diffusion-weighted imaging. AJNR Am J Neuroradiol 2009; 30:64–70. [CrossRef]
7. de Graaf P, Pouwels PJ, Rodjan F, et al. Single-shot turbo spin-echo diffusion-weighted imaging for retinoblastoma: initial experience. AJNR Am J Neuroradiol 2012; 33:110–118. [CrossRef]
8. Politi LS, Forghani R, Godi C, et al. ocular adnexal lymphoma: diffusion-weighted MR imaging for differential diagnosis and therapeutic monitoring. Radiology 2010; 256:565–574. [CrossRef]
9. Sepahdari AR, Kapur R, Aakalu VK, et al. Diffusion-weighted imaging of malignant ocular masses: initial results and directions for further study. AJNR Am J Neuroradiol 2012; 33:314–319. [CrossRef]

10. Sepahdari AR, Aakalu VK, Setabutr P, et al. Indeterminate orbital masses: restricted diffusion at MR imaging with echo-planar diffusion-weighted imaging predicts malignancy. Radiology 2010; 256:554–564. [CrossRef]
11. Lope LA, Hutcheson KA, Khademian ZP. Magnetic resonance imaging in the analysis of pediatric orbital tumors: utility of diffusion-weighted imaging. J AAPOS 2010; 14:257–262. [CrossRef]
12. Razek AA, Elkhamary S, Mousa A. Differentiation between benign and malignant orbital tumors at 3-T diffusion MR imaging. Neuroradiology 2011; 53:517–522. [CrossRef]
13. Ahn SJ, Choi SH, Kim YJ, et al. Histogram analysis of apparent diffusion coefficient map of standard and high B-value diffusion MR imaging in head and neck squamous cell carcinoma: a correlation study with histological grade. Acad Radiol 2012; 19:1233–1240. [CrossRef]
14. Suo ST, Chen XX, Fan Y, et al. Histogram analysis of apparent diffusion coefficient at 3.0 T in urinary bladder lesions: correlation with pathologic findings. Acad Radiol 2014; 21:1027–1034. [CrossRef]
15. Ma X, Zhao X, Ouyang H, et al. Quantified ADC histogram analysis: a new method for differentiating mass-forming focal pancreatitis from pancreatic cancer. Acta Radiol 2014; 55:785–792. [CrossRef]
16. Ryu YJ, Choi SH, Park SJ, et al. Glioma: application of whole-tumor texture analysis of diffusion-weighted imaging for the evaluation of tumor heterogeneity. PLoS One 2014; 9:e108335. [CrossRef]
17. Woo S, Cho JY, Kim SY, et al. Histogram analysis of apparent diffusion coefficient map of diffusion-weighted MRI in endometrial cancer: a preliminary correlation study with histological grade. Acta Radiol 2014; 55:1270–1277. [CrossRef]
18. Cho SH, Kim GC, Jang YJ, et al. Locally advanced rectal cancer: post-chemoradiotherapy ADC histogram analysis for predicting a complete response. Acta Radiol 2015; 56:1042– 1050. [CrossRef]
19. Zhang YD, Wang Q, Wu CJ, et al. The histogram analysis of diffusion-weighted intravoxel incoherent motion (IVIM) imaging for differentiating the gleason grade of prostate cancer. Eur Radiol 2015; 25:994–1004. [CrossRef]
20. Donati OF, Mazaheri Y, Afaq A, et al. Prostate cancer aggressiveness: assessment with whole-lesion histogram analysis of the apparent diffusion coefficient. Radiology 2014; 271:143–152. [CrossRef]
21. Heo SH, Shin SS, Kim JW, et al. Pre-treatment diffusion-weighted MR imaging for predicting tumor recurrence in uterine cervical cancer treated with concurrent chemoradiation: value of histogram analysis of apparent diffusion coefficients. Korean J Radiol 2013; 14: 616–625. [CrossRef]
22. Kim EJ, Kim SH, Park GE, et al. Histogram analysis of apparent diffusion coefficient at 3.0T: Correlation with prognostic factors and subtypes of invasive ductal carcinoma. J Magn Reson Imaging 2015; 42:1666-1678. [CrossRef]
23. Suh CH, Kim HS, Lee SS, et al. Atypical imaging features of primary central nervous system lymphoma that mimics glioblastoma: utility of intravoxel incoherent motion MR imaging. Radiology 2014; 272:504–513. [CrossRef]
24. Tailor TD, Gupta D, Dalley RW, et al. Orbital neoplasms in adults: clinical, radiologic, and pathologic review. Radiographics 2013; 33:1739–1758. [CrossRef]
25. Baek HJ, Kim HS, Kim N, et al. Percent change of perfusion skewness and kurtosis: a potential imaging biomarker for early treatment response in patients with newly diagnosed glioblastomas. Radiology 2012; 264:834–843. [CrossRef]
26. Kang Y, Choi SH, Kim YJ, et al. Gliomas: histogram analysis of apparent diffusion coefficient maps with standard- or high-b-value diffusion-weighted MR imaging--correlation with tumor grade. Radiology 2011; 261:882–890. [CrossRef]
27. Lu SS, Kim SJ, Kim N, et al. Histogram analysis of apparent diffusion coefficient maps for differentiating primary CNS lymphomas from tumefactive demyelinating lesions. AJR Am J Roentgenol 2015; 204:827–834. [CrossRef]